Trajectory Optimization for Constrained UAVs: a Virtual Target Vehicle Approach

Alessandro Rucco, A. Pedro Aguiar, and John Hauser

Abstract— **In this paper we propose a novel approach for trajectory optimization for constrained Unmanned Aerial Vehicles (UAVs). With regard to the classical trajectory optimization problem, we take a Virtual Target Vehicle (VTV) perspective by introducing a virtual target that plays the role of an additional control input. Based on a nonlinear projection operator optimal control technique and extending the concepts of the maneuver regulation framework, we propose a trajectory optimization based strategy to compute, for any given desired path with a specified desired speed profile, the (local) optimal feasible trajectory that best approximates the desired one. The optimization procedure takes explicitly into account the extra flexibility of the VTV by changing (during the transient period) the velocity of the virtual target with the benefit of improving the convergence of the solver to obtain the optimal feasible path, and also avoid the singularities that occur in some maneuver regulation techniques described in the literature. We provide numerical computations for three testing scenarios that illustrates the effectiveness of the proposed strategy.**

I. INTRODUCTION

Unmanned aerial vehicles (UAVs) play an important role in several complex tasks for both civilian and military missions. Interesting scenarios include: search and rescue operations (UAVs have to reach the target with time and space constraints), long endurance missions (UAVs have to harvest energy from the atmospheric flow field to improve their endurance), environmental measurements tasks (cooperative UAVs motion planning allows one to predict flow field phenomena with high precision), see, e.g., [1], [2], and [3]. These missions motivate the computation and execution of optimal maneuvers. Due to the dynamics-constrained nonlinear problems, the computation of such maneuvers for UAVs is specially challenging.

Once the desired UAV motion is computed, the classical approaches used in the literature to make the UAV execute it fall into the categories of trajectory tracking and path following methods. Trajectory tracking methods are concerned with the design of control laws that force a vehicle to reach and follow a time parameterized reference (i.e., a geometric path with an associated timing law), see, e.g., [4], [5], and [6]. In path following methods, the vehicle is required to converge to and follow a path that is specified without a temporal law, see, e.g., [7] and [8]. In [9] the authors provide a comparison in terms of both accuracy and control effort performance among these two and others path-following algorithms for straight line and loiter paths. We refer to [10] and [11] for a comparison and discussion between the trajectory tracking and the path following approaches.

An extended version of path following is the maneuver regulation that aims at satisfying explicitly additional requirements, such as assigning orientation and velocity along the desired path. In [12] a nonlinear controller for aggressive maneuvering of a quadrotor is proposed. It is worth noting that, due to the transverse coordinates, the vehicle is constrained to be inside a tube around the desired path. Based on the motion of a virtual target, a nonlinear controller for UAVs has been developed in [13] to asymptotically follow a smooth reference path. The problem is solved by using a suitable Lyapunov function. The vehicle is not constrained to be inside a tube around the desired path, yet there are no considerations of optimality in the paths to be followed by the UAVs. In [14] a trajectory optimization strategy for vehicles maneuvering is proposed. Motivated by the constrained environment setup, the authors propose the use of the transverse coordinates. In

Alessandro Rucco and A. Pedro Aguiar are with the Research Center for Systems and Technologies, Faculty of Engineering, University of Porto, Porto, Portugal, {alessandrorucco, pedro.aguiar}@fe.up.pt

John Hauser is with the Department of Electrical, Computer, and Energy Engineering, University of Colorado, Boulder, USA, hauser@colorado.edu

this paper, we extend and adapt the trajectory optimization strategy in [14] for UAVs by taking a Virtual Target Vehicle (VTV) perspective where a virtual target is introduced that plays the role of an additional control input.

The contributions of the paper are as follows. We propose a trajectory exploration strategy for aggressive maneuvering of constrained UAVs. Based on the idea described in [15] for underwater vehicles, we set up a constrained optimal problem in terms of longitudinal and lateral tracking error between the actual UAV and the VTV. The proposed strategy explicitly takes into account the velocity of the VTV, which helps to improve the convergence of the actual path to the desired one. Using the projection operator Newton method, [16], combined with the barrier function relaxation developed in [17], we explore the system dynamics of the constrained UAV model. We provide numerical computations to show the effectiveness of the proposed strategy. The numerical computations highlight that the algorithm i) does not suffer from the singularities that occur in some maneuver regulation techniques described in the literature (as, e.g., the one described in [14]), ii) the algorithm exhibits quadratic convergence rate in the neighborhood of the (local) minimum.

The rest of the paper is organized as follows. In Section II, we describe the UAV model for coordinated flight. In Section III we formulate the optimal control problem and its formulation by using the VTV approach. In Section IV we describe the optimal control based strategy to compute feasible trajectories and provide numerical computations based on straight line and loiters maneuvers, and a highly aggressive maneuver.

II. CONSTRAINED UAV MODEL

In this section, we briefly introduce a planar aerial vehicle model in coordinated flight. The vehicle dynamics is based on a simplified model widely used in the literature, see, e.g., [14] and [18]. We assume i) a small angle of attack and ii) the UAV is equipped with an autopilot for low level control. The autopilot forces coordinated turns (i.e., the side slip angle is kept near zero over the entire maneuver) at a fixed altitude. The planar

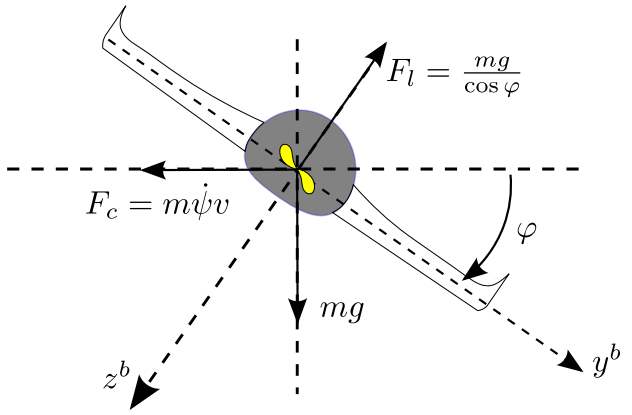

Fig. 1: A fixed wing aircraft executing a coordinated turn at fixed altitude. The origin of the body-frame of the aircraft is located at the center of mass with x^b-y^b-z^b axes oriented in a forward-right-down fashion.

UAV motion can be described by, [14],

$$\begin{aligned}\dot{x} &= v\cos\psi\,,\\ \dot{y} &= v\sin\psi\,,\\ \dot{\psi} &= \frac{a_{lat}}{v}\,,\\ \dot{v} &= a_{lon}\,,\end{aligned}$$

where (x,y) is the longitudinal and lateral position (with respect to the global spatial frame), ψ is the heading angle, v is the airspeed, and a_{lon} and a_{lat} are the longitudinal and lateral acceleration of the UAV center of mass expressed in the velocity frame. Following [13], we extend this model by including a static map for the roll angle φ. The idea is to compute the roll angle by enforcing the lateral equilibrium of the acting forces on the vehicle. This allows us to have a (static) map between the roll angle and the lateral acceleration. For UAVs in coordinated flight, the net side force in the aircraft's body frame is zero and

$$F_c = F_l\sin\varphi\,,$$

where F_c and F_l denote the centrifugal and the lift force, respectively, see Fig. 1. For fixed altitude, the vertical component of lift must continue to equal the weight and, therefore,

$$ma_{lat} = mg\tan\varphi\,,$$

where m and g denote the aircraft's mass and the gravity acceleration, respectively. In the view of the coordinated flight assumption, we can translate

a given lateral acceleration command into a roll angle by using the following static map

$$a_{lat} = g \tan \varphi \,. \tag{1}$$

Moreover, we take into account the roll dynamics and use the roll rate as control input. To sum up, the equations of motion are the following

$$\begin{aligned} \dot{x} &= v \cos \psi \,, \\ \dot{y} &= v \sin \psi \,, \\ \dot{\psi} &= \frac{g \tan \varphi}{v} \,, \\ \dot{v} &= u_1 \,, \\ \dot{\varphi} &= u_2 \,. \end{aligned} \tag{2}$$

The state variables are represented by the position (x,y), the heading angle ψ, the velocity v and the roll angle φ. The longitudinal acceleration $\dot{v}$ and the roll rate $\dot{\varphi}$ are the control inputs. We will refer to the system (2) as Coordinated Flight Vehicle (CFV) to recall the coordinated flight feature. The CFV involves relatively few parameters and thus can be used to verify that the calculations are meaningful.

It is important to point out that, due to physical limitations or security specifications, state and input constraints are imposed on the CFV. In particular, the velocity is bounded by two positive constants v_{min} and v_{max}, the roll angle, the longitudinal acceleration and the roll rate are bounded in module by φ_{max}, u_{1max} and u_{2max}, respectively. The following state-input constraints are taken into account:

$$\begin{aligned} v_{min} \leq v \leq v_{max} \,, \\ |\varphi| \leq \varphi_{max} \,, \\ |u_1| \leq u_{1max} \,, \\ |u_2| \leq u_{2max} \,. \end{aligned} \tag{3}$$

The constraints parameters used in the paper are based on the ones given in [6], i.e., $v_{min} = 18$m/s, $v_{max} = 25$m/s, $\varphi_{max} = 24$deg, $u_{1max} = 0.2$m/s^2, $u_{2max} = 28$deg/s.

III. PROBLEM FORMULATION AND VIRTUAL TARGET APPROACH

In this section we address the problem of computing an optimal trajectory of the CFV model that best approximates a desired maneuver (desired path with a velocity profile assigned on it). We introduce the Virtual Target Vehicle approach and rewrite the CFV model with respect to a new set of coordinates. We provide a rigorous optimal control problem formulation with respect to the new dynamical system.

Given a desired geometric path $(\bar{x}_{des}(s), \bar{y}_{des}(s))$ parameterized by the variable $s \in \mathbb{R}$ and the initial condition of the CFV, our goal is to obtain a feasible trajectory (i.e., it must satisfy the dynamics of the nonlinear system (2) and the constraints (3)) that accurately tracks the desired path with a specified desired velocity along the path $\bar{v}_{des}(s)$. To this end, one approach is to use the optimization strategy proposed in [14] which unfolds in the computation of i) the distance between the origin of the body-frame and the "closest point" on the path (i.e., the projection of the actual vehicle on the desired path), and ii) the angle between the vehicle's total velocity vector and the tangent to the path at the (computed) closest point. The goal is to reduce both to zero. In this paper, contrary to [14] where the Serret-Frenet frame is attached to the point on the path that is closest to the vehicle, we do not impose this restriction. The Serret-Frenet frame, which can be viewed as the body frame of a "Virtual Target Vehicle" that should be tracked by the actual vehicle, moves along the desired path according to a "conveniently velocity", effectively yielding an extra control input.

Following this idea, consider a Virtual Target Vehicle (VTV) that is constrained to travel along the desired path, see Fig. 2. Given the arc-length parametrization of the VTV path, $s_{vtv} \mapsto (\bar{x}_{vtv}(s_{vtv}), \bar{y}_{vtv}(s_{vtv}))$, we choose a new set of coordinates. Note that the bar symbol indicates that a quantity is expressed as a function of the arc-length rather than time. The coordinates of the CFV (x,y) can be defined with respect to the position of the VTV, see Fig. 2,

$$\begin{bmatrix} x \\ y \end{bmatrix} = \begin{bmatrix} \bar{x}_{vtv} \\ \bar{y}_{vtv} \end{bmatrix} + R_z(\bar{\chi}_{vtv}) \begin{bmatrix} w_1 \\ w_2 \end{bmatrix} , \tag{4}$$

where w_1 and w_2 are the longitudinal and lateral error coordinates, respectively, and

$$R_z(\bar{\chi}_{vtv}) = \begin{bmatrix} \cos \bar{\chi}_{vtv} & -\sin \bar{\chi}_{vtv} \\ \sin \bar{\chi}_{vtv} & \cos \bar{\chi}_{vtv} \end{bmatrix}$$

is the rotation matrix transforming vectors from the error frame into the global spatial frame.

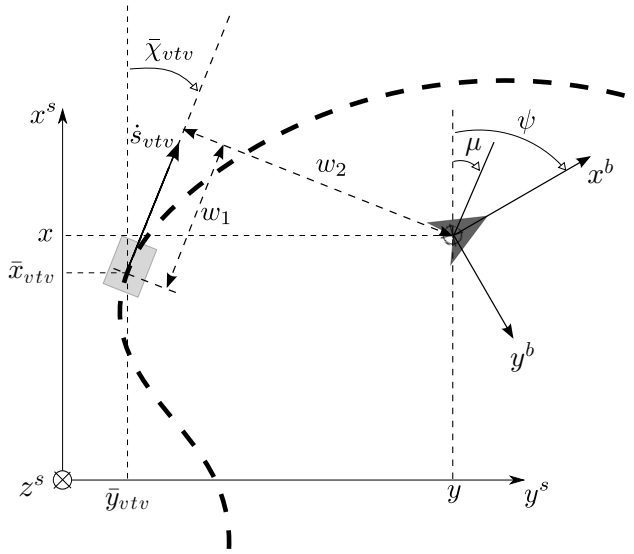

Fig. 2: Tracking error coordinates. The bold triangle and the light rectangle indicate the real UAV and the VTV, respectively. The bold dash line indicates the desired path.

From now on, we use a prime symbol to denote the first derivative of a variable with respect to the arc-length s_{vtv}. For example, $\bar{x}'(s_{vtv}) = \frac{d\bar{x}(s_{vtv})}{ds_{vtv}}$, while $\dot{x}(t) = \frac{dx(t)}{dt}$. Next, we compute the expression of $\dot{w}_1$ and $\dot{w}_2$. To this end, we differentiate (4) with respect to the time t, and we get

$$\begin{aligned}\begin{bmatrix} \dot{x} \\ \dot{y} \end{bmatrix} =& \begin{bmatrix} \bar{x}'_{vtv} \\ \bar{y}'_{vtv} \end{bmatrix} \dot{s}_{vtv} \\ &+ \begin{bmatrix} -\sin\bar{\chi}_{vtv} & -\cos\bar{\chi}_{vtv} \\ \cos\bar{\chi}_{vtv} & -\sin\bar{\chi}_{vtv} \end{bmatrix} \begin{bmatrix} w_1 \\ w_2 \end{bmatrix} \bar{\sigma}_{vtv}\dot{s}_{vtv} \\ &+ R_z(\bar{\chi}_{vtv}) \begin{bmatrix} \dot{w}_1 \\ \dot{w}_2 \end{bmatrix}.\end{aligned}$$

Taking into account that the course heading $\bar{\chi}_{vtv}$ and curvature $\bar{\sigma}_{vtv}$ are related by differentiation,

$$\begin{aligned}\bar{x}'_{vtv} &= \cos\bar{\chi}_{vtv} \\ \bar{y}'_{vtv} &= \sin\bar{\chi}_{vtv} \\ \bar{\chi}'_{vtv} &= \bar{\sigma}_{vtv}\end{aligned}$$

and using the kinematic of the CFV model (2), we have

$$\begin{aligned}R_z(\psi) \begin{bmatrix} v \\ 0 \end{bmatrix} =& R_z(\bar{\chi}_{vtv}) \begin{bmatrix} \dot{s}_{vtv} \\ 0 \end{bmatrix} \\ &- R_z(\bar{\chi}_{vtv}) \begin{bmatrix} w_2 \\ -w_1 \end{bmatrix} \bar{\sigma}_{vtv}\dot{s}_{vtv} \\ &+ R_z(\bar{\chi}_{vtv}) \begin{bmatrix} \dot{w}_1 \\ \dot{w}_2 \end{bmatrix},\end{aligned}$$

that is

$$\begin{bmatrix} (1-w_2\bar{\sigma}_{vtv})\dot{s}_{vtv} + \dot{w}_1 \\ w_1\bar{\sigma}_{vtv}\dot{s}_{vtv} + \dot{w}_2 \end{bmatrix} = R_z(\bar{\chi}_{vtv})^T R_z(\psi) \begin{bmatrix} v \\ 0 \end{bmatrix}.$$

Now it is straightforward to compute the expression of $\dot{w}_1$ and $\dot{w}_2$ as

$$\begin{aligned}\dot{w}_1 &= v\cos(\psi - \bar{\chi}_{vtv}) - (1-w_2\bar{\sigma}_{vtv})\dot{s}_{vtv}, \\ \dot{w}_2 &= v\sin(\psi - \bar{\chi}_{vtv}) - w_1\bar{\sigma}_{vtv}\dot{s}_{vtv}.\end{aligned} \tag{5}$$

Defining the local heading angle as $\mu = \psi - \bar{\chi}_{vtv}$ and the VTV's velocity as an additional control input $u_3 = \dot{s}_{vtv}$, the nonlinear system (2) can be written with respect to the new set of coordinates $(\mathbf{x}, \mathbf{u}) = (w_1, w_2, \mu, v, \varphi, s_{vtv}, u_1, u_2, u_3)$:

$$\begin{aligned}\dot{w}_1 &= v\cos\mu - (1-w_2\bar{\sigma}_{vtv})u_3, \\ \dot{w}_2 &= v\sin\mu - w_1\bar{\sigma}_{vtv}u_3, \\ \dot{\mu} &= \frac{g\tan\varphi}{v} - \bar{\sigma}_{vtv}u_3, \\ \dot{v} &= u_1, \\ \dot{\varphi} &= u_2, \\ \dot{s}_{vtv} &= u_3.\end{aligned} \tag{6}$$

Remark 3.1: It is worth noting that in [14] $w_1 = 0$ for all t, because the point on the desired path is defined by the projection of the actual vehicle on the path. In such a case, the velocity of the virtual target is given by

$$\dot{s}_{vtv} = \frac{v\cos\mu}{1-\bar{\sigma}_{vtv}w_2},$$

and a singularity appears at $w_2 = \frac{1}{\bar{\sigma}_{vtv}}$. Such a singularity constrains the position of the actual vehicle to be inside a "tube" around the desired path. This constraint is very conservative and can affect the exploration of trajectories of the vehicle. In this paper, we explicitly take into account the velocity of the virtual target (as a new control input) thus removing such singularity. □

We now address the problem of exploring system trajectories (maneuvers) by using nonlinear least squares trajectory optimization. That is, we consider the following optimal control problem

$$\begin{aligned}\min_{\mathbf{x}(\cdot),\mathbf{u}(\cdot)} \frac{1}{2}\int_0^T \|\mathbf{x}(\tau)-\mathbf{x}_d(\tau)\|_Q^2 + \|\mathbf{u}(\tau)-\mathbf{u}_d(\tau)\|_R^2 dt \\ + \frac{1}{2}\|\mathbf{x}(T)-\mathbf{x}_d(T)\|_{P_1}^2 \\ \text{subj. to (6), } \texttt{dynamics constraints} \\ \text{(3), } \texttt{state/input constraints}\end{aligned} \tag{7}$$

where $(\mathbf{x}_d(\cdot),\mathbf{u}_d(\cdot))$ is a desired curve, $T>0$ is fixed, and Q, R and P_1 are positive definite weighting matrices such that, for $z\in\mathbb{R}^n$ and $W\in\mathbb{R}^{n\times n}$, $\|z\|^2_W = z^T W z$.

Remark 3.2: The goal is to compute the optimal trajectory that is close in the L_2 norm to the desired maneuver (path and velocity). For this reason, the desired kinematic coordinates, w_{1des}, w_{2des}, and μ_{des}, are set to zero. The desired velocity, v_{des}, and the desired length, s_{des}, are assigned. The other remaining states and the inputs are chosen as follow. Given v_{des} and σ_{des}, the desired roll angle is set to be $\varphi_{des} = \arctan\frac{v_{des}^2\sigma_{des}}{g}$ (by inverting the static map (1)). The desired velocity of the VTV, u_{3des}, is set to be equal to v_{des}. Finally, in order to take into account a penalty on the control effort, the desired longitudinal acceleration and roll rate, u_{1des} and u_{2des}, are set to zero. □

IV. TRAJECTORY EXPLORATION

In this section we describe the optimal control based strategy used to explore the trajectory manifold of the CFV introduced in the previous section and provide numerical computations showing its effectiveness.

A. Optimization of trajectory functionals with constraints

We recall that a trajectory is a (state-input) curve $\eta = (\mathbf{x}(\cdot),\mathbf{u}(\cdot))$ defined on $L_\infty[0,T]$ such that

$$\dot{\mathbf{x}}(t) = f(\mathbf{x}(t),\mathbf{u}(t)),$$

for all $t\in[0,T]$, where $f:\mathbb{R}^6\times\mathbb{R}^3\longrightarrow\mathbb{R}^6$ and $f\in\mathscr{C}^r$ with $0\le r\le\infty$. Consider now the cost functional

$$h(\xi) = \frac{1}{2}\int_0^T \|\mathbf{x}(\tau)-\mathbf{x}_d(\tau)\|^2_Q + \|\mathbf{u}(\tau)-\mathbf{u}_d(\tau)\|^2_R dt + \frac{1}{2}\|\mathbf{x}(T)-\mathbf{x}_d(T)\|^2_{P_1}$$

and denote by $\mathscr{T}$ the manifold of bounded trajectories $\xi=(\mathbf{x}(\cdot),\mathbf{u}(\cdot))$ on $[0,T]$.

Based on the idea developed in [17], we use a barrier function relaxation to handle the constraints. In order to have a smooth function defining the constraints (3), we rewrite them in the equivalent form

$$c_1(v(t)) = \left(\frac{v(t)-(v_{max}+v_{min})}{v_{max}-v_{min}}\right)^2 - 1 \le 0,$$

$$c_2(\varphi(t)) = \left(\frac{\varphi(t)}{\varphi_{max}}\right)^2 - 1 \le 0,$$

$$c_3(u_1(t)) = \left(\frac{u_1(t)}{u_{1max}}\right)^2 - 1 \le 0,$$

$$c_4(u_2(t)) = \left(\frac{u_2(t)}{u_{2max}}\right)^2 - 1 \le 0,$$

$\forall t\in[0,T]$. For a given (state-input) trajectory $\xi = (\mathbf{x}(\cdot),\mathbf{u}(\cdot))$, a barrier functional can be defined as

$$b_\delta(\xi) = \int_0^T \Sigma_j \beta_\delta(-c_j(\mathbf{x}(\tau),\mathbf{u}(\tau)))d\tau, j=1,\dots,4,$$

where

$$\beta_\delta(x) = \begin{cases} -\log x, & x>\delta \\ \frac{k-1}{k}\left[\left(\frac{x-k\delta}{(k-1)\delta}\right)^k - 1\right] - \log\delta, & x\le\delta \end{cases}.$$

Using the barrier functional defined above, the relaxed version of problem (7) is given by

$$\min_{\xi\in\mathscr{T}} h(\xi) + \varepsilon b_\delta(\xi), \tag{8}$$

for some $\varepsilon>0$. Using the projection operator defined in [16] to locally parametrize the trajectory manifold, we may convert the constrained optimization problem (8) into one of minimizing the unconstrained functional

$$g_{\varepsilon,\delta}(\xi) = h(\mathscr{P}(\xi)) + \varepsilon b_\delta(\mathscr{P}(\xi)). \tag{9}$$

The PRojection Operator based Newton method for Trajectory Optimization (`PRONTO`), [16], is used to optimize the functional (9), as part of a continuation method to seek an approximate solution to (8). The strategy is to start with a reasonably large ε and δ. Then, for the current ε and δ, the problem

$$\min g_{\varepsilon,\delta}(\xi) \tag{10}$$

is solved using the `PRONTO` method starting from the current trajectory.

Notice that this method has been effectively applied to compute minimum-time trajectories of race cars. We refer the reader to [19] and [20] for more details about the optimal control based strategy.

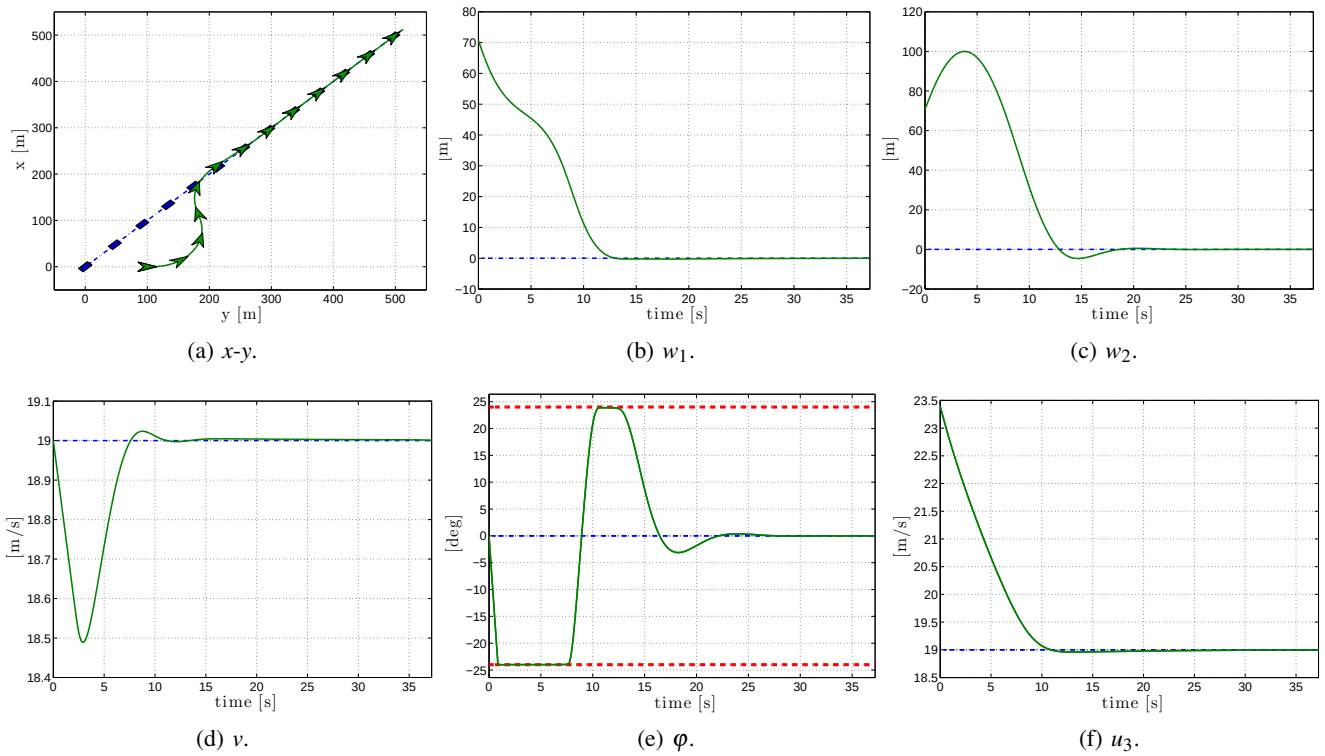

(a) x-y. (b) w_1. (c) w_2.

(d) v. (e) φ. (f) u_3.

Fig. 3: Straight line maneuver. The desired (dash-dot line) and the optimal (solid line) trajectories are shown. The path, the longitudinal and lateral tracking error profiles are shown in (a), (b), and (c), respectively. The velocity, roll angle, and virtual target velocity profiles are shown in (d), (e), and (f), respectively (constraints in dash line).

B. Numerical computations.

1) The straight line maneuver: given the initial position $(x,y) = (0,100)$ and orientation $\psi = \frac{\pi}{2}$ of the actual vehicle, the goal is to approach the desired straight line path (dash line in Fig. 3a) with a desired velocity along it (dash line in Fig. 3d). We run the trajectory exploration strategy by setting the following weighting matrices $Q = diag([0.01, 0.01, 0.1, 1, 0.1, 1e-06])$, $R = diag([0.1, 0.1, 0.1])$.

The algorithm shows a quadratic convergence rate (we recall that the PRONTO has a structure that resembles a standard Newton method) and the optimal trajectory is shown in Fig. 3. Due to the initial position, the CFV turns left (counter-clockwise direction) by applying the maximum roll angle (see Fig. 3e) and, therefore, the maximum lateral acceleration. At the same time, the vehicle decelerates to increase the yaw rate, see Fig. 3d. Thus, for a fixed lateral acceleration, decreasing the velocity allows the vehicle to increase the yaw rate (thus improving the convergence of the actual path to the desired straight line path). It is worth noting that the VTV starts with a high initial velocity (i.e., 23.3m/s) and immediately decelerates (in order to reach the desired one, i.e., $v_{des} = 19$m/s). This initial velocity of the VTV allows the actual vehicle to decrease the longitudinal tracking error w_1, see Fig. 3b. At about $t = 9$sec, the actual vehicle starts to turn on the right (clockwise direction) by applying the maximum (positive) roll angle, see Fig. 3e. It is interesting to note that, at time $t = 10$sec, both VTV and CFV have reached the desired velocity. Now the VTV (slightly) decelerates and the CFV (slightly) accelerates thus approaching the desired maneuver. The CFV crosses the desired straight line at about $(x,y) = (190,190)$ and, in order to regain the desired position, it turns to the right by applying a negative roll angle.

Since the VTV velocity is a fictitious control input, it is interesting to investigate how the weighting matrices in the performance index (7) affects the optimal trajectory. We choose the following weighting matrices

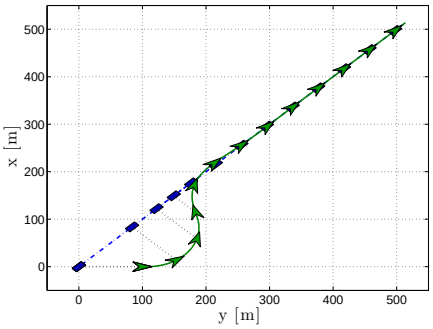

(a) x-y.

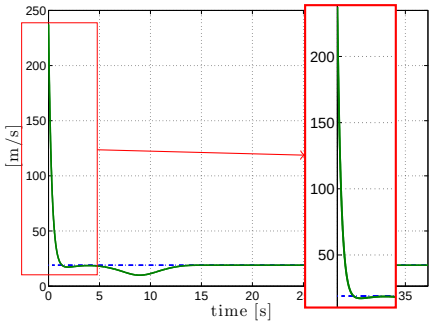

(b) u_3.

Fig. 4: Straight line maneuver, $R(3,3) = 0.0001$, $(x_{vtv}(0), y_{vtv}(0)) = (0,0)$. In (a) the light dot black line represents the tracking error.

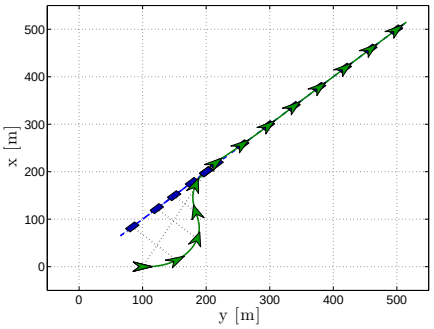

(a) x-y.

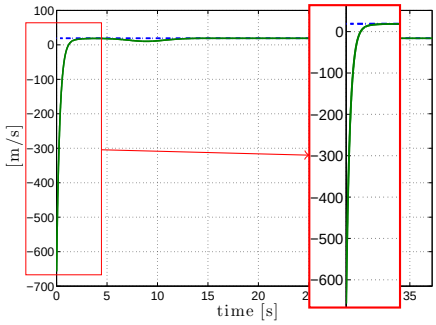

(b) u_3.

Fig. 5: Straight line maneuver, $R(3,3) = 0.0001$, $(x_{vtv}(0), y_{vtv}(0)) = (200,200)$. In (a)the light dot black line represents the tracking error.

$Q = diag([0.01, 0.01, 0.1, 1, 0.1, 1e-06])$, $R = diag([0.1, 0.1, 0.0001])$. In other words, the VTV velocity is weighted lightly thus giving the optimization the necessary freedom to track the states. The optimal trajectory is shown in Fig. 4. As we can see in the zoom-in of Fig. 4b, the VTV velocity has a peak value at $t = 0$. This allows the VTV to decrease (almost instantaneously) the longitudinal tracking error w_1, see Fig. 4a.

Observed this interesting behavior of the VTV, we investigate how the initial position of VTV affects the optimal trajectory. We compute the optimal trajectory by setting $(x_{vtv}(t=0), y_{vtv}(t=0) = (200,200))$. We do not observe substantial differences in the optimal trajectory of the actual vehicle. On the other hand, the VTV assumes a high negative velocity value, see Fig. 5b. It goes backward along the straight line thus approaching (almost instantaneously) the point on the desired path at minimum distance from the CFV position, see Fig. 5a. In this view, the numerical computations highlight important features of the CFV optimal trajectory (it seems to be not affected by the initial position of the VTV) that deserve further theoretical investigation.

2) The loiter maneuver: this maneuver is a circular path with fixed radius (and altitude reference). Usually, it is performed by UAVs for i) surveillance/monitoring missions (i.e., loitering around a desired waypoint) and ii) standby safety mode (e.g., the vehicle executes the loiter while waiting for new tasks). Similarly to the computations shown in [9], we set as desired curve the circular path centered at the origin with a radius of 100m. The desired velocity is 19m/s. The initial CFV position is $(x,y) = (0,125)$, with orientation $\psi = \frac{\pi}{2}$, and velocity $v = 19$m/s. The weighting matrices in the performance index (7) are $Q = diag([0.01, 0.01, 0.1, 1, 0.1, 1e-06])$, $R = diag([0.1, 0.1, 0.0001])$.

In Fig. 6 the optimal trajectory is shown. As observed for the straight line maneuver, the CFV decelerates (see Fig. 6d) to increase the yaw rate and, therefore, its path curvature. The vehicle is turing in the counterclockwise direction and the maximum roll angle is applied (see Fig. 6e). It is worth noting that the constraint on the velocity is active for $t \in [5,7]$sec. Then the CFV accelerates,

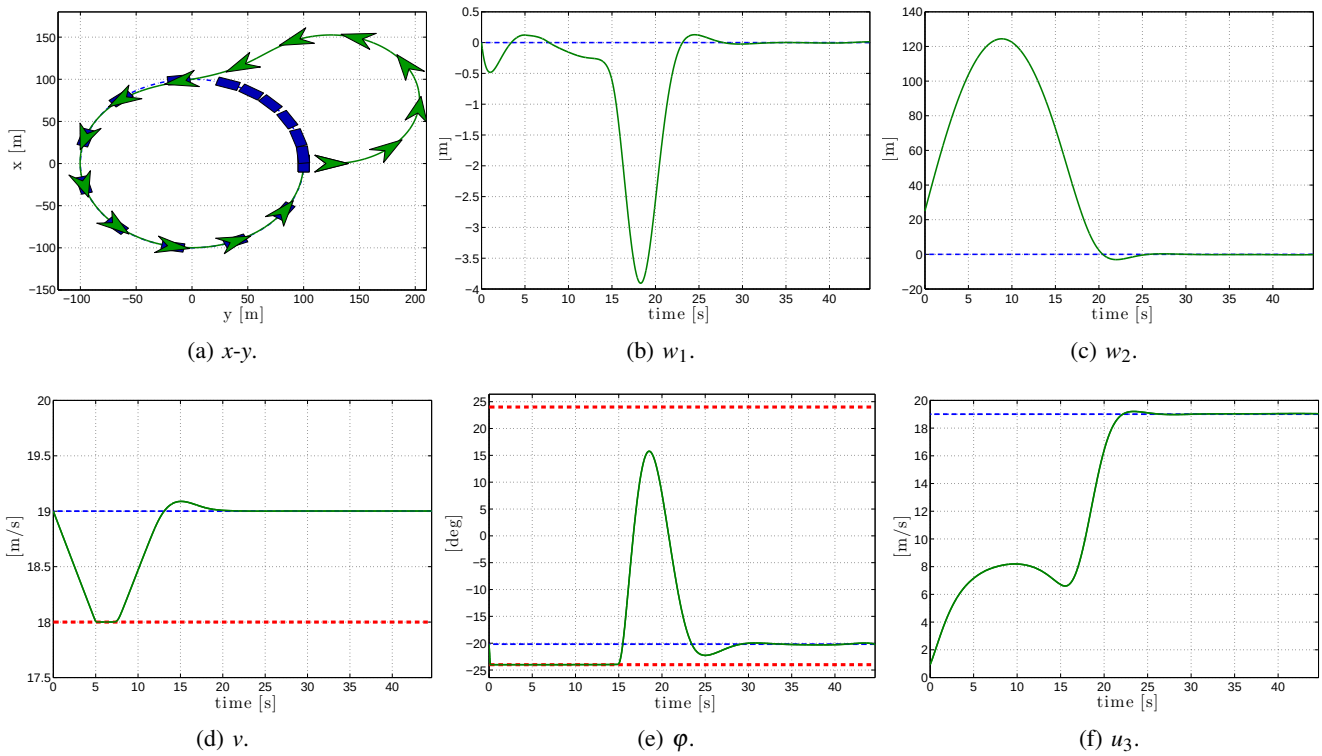

(a) x-y. (b) w_1. (c) w_2.

(d) v. (e) φ. (f) u_3.

Fig. 6: Loiter maneuver. The desired (dash-dot line) and the optimal (solid line) trajectories are shown. The path, the longitudinal and lateral tracking error profiles are shown in (a), (b), and (c), respectively. The velocity, roll angle, and virtual target velocity profiles are shown in (d), (e), and (f), respectively (constraints in dash line).

applies a sharp variation in the roll angle (i.e., it becomes positive and again negative) and approaches the desired maneuver. In contrast to the previous computation, the VTV starts the maneuver with a (very) low velocity, i.e., $u_3 = 1$m/s, see Fig. 6f (note that the VTV velocity is weighted lightly in the performance index). Roughly speaking, the VTV is "waiting" the CFV while it is performing an aggressive maneuver (i.e., it is performing a manevuer at the maximum of its capabilities). Such a (low) velocity allows us to improve the convergence of the actual path to the desired one.

We want to highlight two important features. First, at time $t = 0$ the actual vehicle is oriented along the y-axis. Indeed, the local heading angle is $\mu(t = 0) = \frac{\pi}{2}$. Such a trajectory cannot be explored and performed by using the transverse coordinates. Thus, the dynamics of the vehicle taken into account in [14] has a singularity at $\mu = \pm\frac{\pi}{2}$. Second, by increasing the weighting term in (7) related to the VTV velocity, the ability of the actual vehicle to follow (track) the desired path decreases. In Fig. 7 we show the optimal trajectory obtained by setting $R(3,3) = 0.1$. As we can see in Fig. 7b, the VTV velocity profile is close to the desired one and (in order to track the VTV) the CFV decreases its path curvature thus following almost a straight line (see Fig. 7a, from $(x,y) = (150,100)$ to $(x,y) = (70,-30)$).

3) An aggressive maneuver: as an application on a more complex scenario, the optimal trajectory based on the desired path shown in Fig. 8a (see the dash-dot line) is computed. The desired path consists of two straights and four (sharp) 90 degree turns. The desired velocity along the path is 22m/s. The initial position, orientation and velocity are $(x,y) = (30,0)$, $\psi = \frac{\pi}{4}$ and $v = 20$, respectively. It is worth noting that, due to the desired velocity and the sharp turns, the desired roll angle is unfeasible, see the dash-dot line in Fig. 8c.

The optimal trajectory (solid line) is shown in Fig. 8. Due to the initial velocity, the vehicle starts the maneuver by applying the maximum longitudinal acceleration (the velocity is increasing with its maximum slope, Fig. 8b). Moreover, due to the initial orientation (i.e., $\psi(0) = \frac{\pi}{4}$) and the

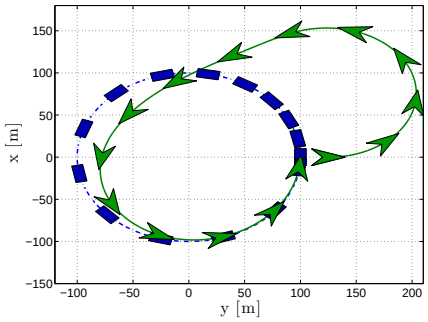

(a) x-y.

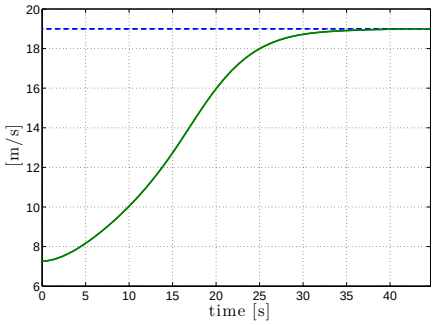

(b) u_3.

Fig. 7: Loiter maneuver, $R(3,3) = 0.1$.

dynamic-constrained problem (i.e., the CFV is a non-holonomic vehicle), the vehicle moves away from the desired path, Fig. 8a. Indeed, the maximum roll angle is applied (Fig. 8c) and the vehicle turns to the right. In this way, the orientation of the vehicle increases (the vehicle is turning clockwise) and it approaches the desired orientation, that is $\frac{\pi}{2}$. Note that, for $t \in [1,6]$s, the vehicles is traveling in steady-state fashion. Thus, the roll angle is constant and it is at the boundary limit, see Fig. 8c. Once the desired path is approached, the vehicle has to deal with two sharp turns. In order to minimize the tracking error and track the desired velocity, the vehicle decreases its path curvature by decreasing the roll angle (while maintaing a constant velocity). However, in the middle of the maneuver, the roll angle is maximum, see Fig. 8c. Then the vehicle moves back to the straight line while maintaing the desired velocity. We want to stress that, although the desired roll angle is unfeasible, the optimization strategy computes a roll angle profile satisfying the constraint, see Fig. 8c.

Finally, we highlight that the desired path includes two turns with radius of 15m. These two turns limit the exploration strategy proposed in [14]. As highlighted in Remark 3.1, by using the transverse coordinates, the vehicle is constrained to be inside a "tube" (with radius 15m) around the desired path. Fig. 8a shows the envelope (in solid gray line) defined by the constraint imposed in [14]. This scenario allows us to strengthen the importance of the VTV approach. Thus, the actual (optimal) path followed by the vehicle is outside the tube, see the zoom-in of Fig. 8a.

We encourage the reader to watch the video attachments corresponding to the discussed numerical computations [21].

V. Conclusions

In this paper we proposed a virtual target vehicle approach for trajectory exploration of constrained UAVs. This approach helps us to overcome some drawbacks that affect (and restrict) the use of transverse coordinates. Based on nonlinear optimal control techniques, we provided an optimization strategy to explore the trajectories of the UAV model. The results show that we are able to i) compute aggressive maneuvers (several constraints are active during the maneuver) and ii) capture interesting features of the planar coordinated flight vehicle.

References

[1] A. Ryan and J. K. Hedrick, "A mode-switching path planner for uav-assisted search and rescue," in *IEEE Conf. on Decision and Control*, 2005, pp. 1471–1476.

[2] R. Bencatel, P. Kabamba, and A. Girard, "Perpetual dynamic soaring in linear wind shear," *AIAA Journal of Guidance, Control, and Dynamics*, vol. 37, no. 5, pp. 1712–1716, 2014.

[3] I. Kaminer, E. Xargay, V. Cichella, N. Hovakimyan, A. M. Pascoal, A. P. Aguiar, V. Dobrokhodov, and R. Ghabcheloo, "Time-critical cooperative path following of multiple uavs: Case studies," in *Advances in Estimation, Navigation, and Spacecraft Control*. Springer, 2015, pp. 209–233.

[4] W. Ren and R. W. Beard, "Trajectory tracking for unmanned air vehicles with velocity and heading rate constraints," *IEEE Transactions on Control Systems Technology*, vol. 12, no. 5, pp. 706–716, 2004.

[5] E. P. Anderson, R. W. Beard, and T. W. McLain, "Real-time dynamic trajectory smoothing for unmanned air vehicles," *IEEE Transactions on Control Systems Technology*, vol. 13, no. 3, pp. 471–477, 2005.

[6] I. Prodan, S. Olaru, R. Bencatel, J. B. De Sousa, C. Stoica, and S.-I. Niculescu, "Receding horizon flight control for trajectory tracking of autonomous aerial vehicles," *Control Engineering Practice*, vol. 21, no. 10, pp. 1334–1349, 2013.

[7] A. Ratnoo, P. Sujit, and M. Kothari, "Adaptive optimal path following for high wind flights," in *IFAC World Congress*, 2011.

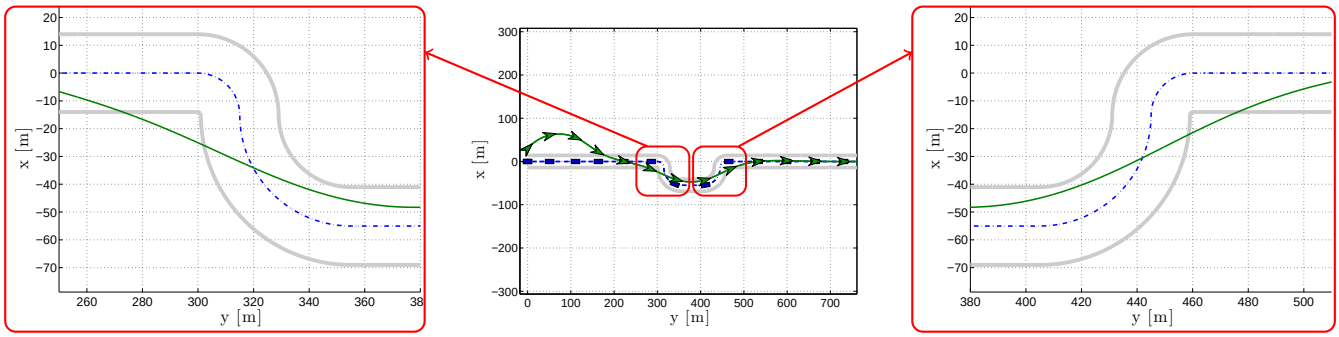

(a) x-y.

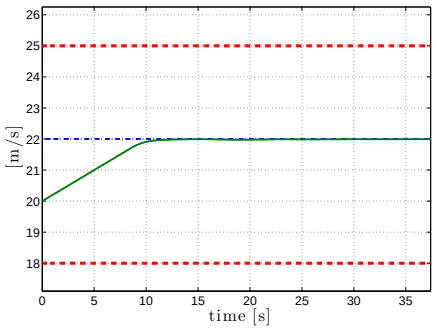

(b) v.

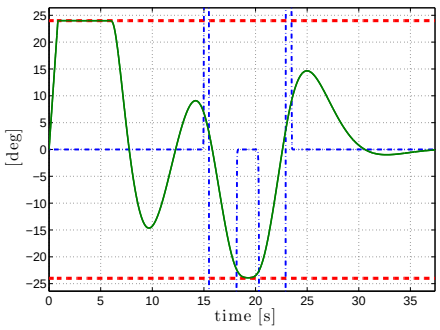

(c) φ.

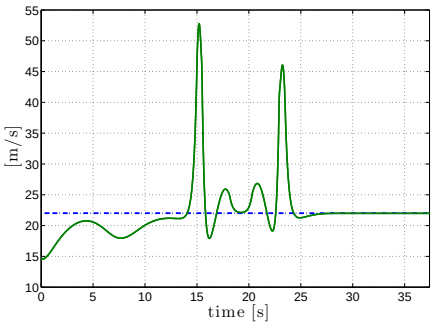

(d) u_3.

Fig. 8: Aggressive maneuver. The desired (dash-dot line) and the optimal (solid line) trajectories are shown. The path, velocity, roll angle, and virtual target velocity profiles are shown in (a), (b), (c), and (d), respectively (constraints in dash line). The grey lines in (a) show the envelope defined by the lateral constraint imposed in [14]. We highlight that the optimal path lies outside the tube around the path, see the zoom-in in (a).

[8] D. R. Nelson, D. B. Barber, T. W. McLain, and R. W. Beard, "Vector field path following for miniature air vehicles," *IEEE Transactions on Robotics*, vol. 23, no. 3, pp. 519–529, 2007.

[9] P. Sujit, S. Saripalli, and J. Sousa, "Unmanned aerial vehicle path following: A survey and analysis of algorithms for fixed-wing unmanned aerial vehicless," *IEEE Control Systems Magazine*, vol. 34, no. 1, pp. 42–59, 2014.

[10] A. P. Aguiar and J. P. Hespanha, "Trajectory-tracking and path-following of underactuated autonomous vehicles with parametric modeling uncertainty," *IEEE Transactions on Automatic Control*, vol. 52, no. 8, pp. 1362–1379, 2007.

[11] A. P. Aguiar, J. P. Hespanha, and P. V. Kokotović, "Performance limitations in reference tracking and path following for nonlinear systems," *Automatica*, vol. 44, no. 3, pp. 598–610, 2008.

[12] S. Spedicato, G. Notarstefano, H. H. Bülthoff, and A. Franchi, "Aggressive maneuver regulation of a quadrotor uav," in *The 16th International Symposium on Robotics Research*, 2013, pp. 1–16.

[13] G. Flores, I. Lugo-Cárdenas, and R. Lozano, "A nonlinear path-following strategy for a fixed-wing mav," in *International Conference on Unmanned Aircraft Systems*, 2013, pp. 1014–1021.

[14] F. Bayer and J. Hauser, "Trajectory optimization for vehicles in a constrained environment." in *IEEE Conf. on Decision and Control*, 2012, pp. 5625–5630.

[15] L. Lapierre, D. Soetanto, and A. Pascoal, "Nonlinear path following with applications to the control of autonomous underwater vehicles," in *IEEE Conf. on Decision and Control*, 2003, pp. 1256–1261.

[16] J. Hauser, "A projection operator approach to the optimization of trajectory functionals," in *IFAC World Congress*, 2002.

[17] J. Hauser and A. Saccon, "A barrier function method for the optimization of trajectory," in *IEEE Conf. on Decision and Control*, 2006, pp. 864–869.

[18] J. Hauser and R. Hindman, "Aggressive flight maneuvers," in *IEEE Conf. on Decision and Control*, 1997, pp. 4186–4191.

[19] A. Rucco, G. Notarstefano, and J. Hauser, "Computing minimum lap-time trajectories for a single-track car with load transfer," in *IEEE Conf. on Decision and Control*, 2012, pp. 6321–6326.

[20] ——, "An efficient minimum-time trajectory generation strategy for two-track car vehicles," *IEEE Transactions on Control Systems Technology*, February 2015.

[21] [Online]. Available: http://youtu.be/WyIkJsqNWyI